Research Article

Hysteresis-Free, High-Performance Polymer-Dielectric Organic Field-Effect Transistors Enabled by Supercritical Fluid

Yuhao Shi [iD],[1] **Yingkai Zheng,**[2] **Jialiang Wang,**[1] **Ran Zhao,**[1] **Tao Wang,**[1] **Changbin Zhao,**[1] **Kuan-Chang Chang** [iD],[2] **Hong Meng,**[1] and **Xinwei Wang**[1]

[1]*School of Advanced Materials, Shenzhen Graduate School, Peking University, Shenzhen 518055, China*
[2]*School of Electronic and Computer Engineering, Shenzhen Graduate School, Peking University, Shenzhen 518055, China*

Correspondence should be addressed to Hong Meng; menghong@pku.edu.cn and Xinwei Wang; wangxw@pkusz.edu.cn

Organic field-effect transistors (OFETs) are of the core units in organic electronic circuits, and the performance of OFETs replies critically on the properties of their dielectric layers. Owing to the intrinsic flexibility and natural compatibility with other organic components, organic polymers, such as poly(vinyl alcohol) (PVA), have emerged as highly interesting dielectric materials for OFETs. However, unsatisfactory issues, such as hysteresis, high subthreshold swing, and low effective carrier mobility, still considerably limit the practical applications of the polymer-dielectric OFETs for high-speed, low-voltage flexible organic circuits. This work develops a new approach of using supercritical CO_2 fluid (SCCO$_2$) treatment on PVA dielectrics to achieve remarkably high-performance polymer-dielectric OFETs. The SCCO$_2$ treatment is able to completely eliminate the hysteresis in the transfer characteristics of OFETs, and it can also significantly reduce the device subthreshold slope to 0.25 V/dec and enhance the saturation regime carrier mobility to 30.2 cm^2 V^{-1} s^{-1}, of which both the numbers are remarkable for flexible polymer-dielectric OFETs. It is further demonstrated that, coupling with an organic light-emitting diode (OLED), the SCCO$_2$-treated OFET is able to function very well under fast switching speed, which indicates that an excellent switching behavior of polymer-dielectric OFETs can be enabled by this SCCO$_2$ approach. Considering the broad and essential applications of OFETs, we envision that this SCCO$_2$ technology will have a very broad spectrum of applications for organic electronics, especially for high refresh rate and low-voltage flexible display devices.

1. Introduction

Organic electronic devices have recently aroused great attention for their high mechanical flexibility and low fabrication cost with diverse important functionalities [1–4]. In organic circuits, organic field-effect transistors (OFETs) are of the core units, which are essential for a huge number of practical applications, such as flexible displays [5, 6], radiofrequency identification tags [7, 8], wearable sensors [9, 10], and biocompatible devices [11, 12]. The performance of the OFET devices replies critically on the properties of the dielectric layers in them. For instance, the polarization, purity, and charge traps of the dielectrics strongly affect the hysteresis, subthreshold swing, leakage and on/off currents, and effective carrier mobility of OFETs, thereby affecting the switching speed, power consumption, and stability of the organic circuits [13–16]. Moreover, the mechanical properties of

the dielectrics are also very important, especially for flexible applications such as rollable displays [17, 18]. The materials of the dielectrics for OFETs are often inorganic oxides, organic polymers, and their mixtures or multilayers [13]. Among these materials, the organic polymer dielectrics are of particular interest, because they are intrinsically flexible and also naturally compatible with other organic components in devices [14, 19]. These merits are particularly important for flexible applications, such as rollable displays, where bending the devices down to <1 mm in radius is required and the inorganic dielectrics are difficult to meet this requirement [18, 20–22].

As a representative polymer dielectric, poly(vinyl alcohol) (PVA) is of particularly common interest for the use in OFETs [22–25]. PVA has a simple structure and of low manufacturing cost, and it also has a relatively high dielectric constant and can be easily spin-coated to afford

films. However, PVA contains moisture-sensitive hydroxyl groups, which can act as electron traps causing issues of hysteresis, leakage, and stability for OFETs [26, 27], and also sodium impurities (hundreds ppm level) are almost inevitable in PVA because NaOH is used in the synthesis of PVA from hydrolyzing poly(vinyl acetate) [15, 28, 29]. Previous works showed that the dielectric performance of PVA could be improved by UV irradiation or annealing in air with a cross-linking agent such as ammonium dichromate or glutaraldehyde [22–24, 30], but this approach is not very effective in removing the hydroxyls and apparently it cannot remove the ionic impurities in PVA. Consequently, the device performance such as hysteresis, subthreshold swing, and effective carrier mobility is still not satisfactory, which considerably limits the practical applications of the polymer-dielectric OFETs for high-speed, low-voltage flexible organic circuits.

In this work, we develop a new approach of using a supercritical CO_2 fluid ($SCCO_2$) to treat PVA to boost its dielectric performance. Supercritical fluids have combined properties of vapor and liquid; their densities and viscosities are lower than liquids and their diffusivities are high like gases, so the transfer of mass in supercritical fluids is very rapid [31–33]. With an additive of desiccant, such as anhydrous calcium chloride, the supercritical CO_2 fluid can remove water and other impurities in a fast and efficient way [34–36]. As demonstrated in the following, benefited from the merits of the supercritical fluids, the dielectric performance of PVA is significantly boosted by the $SCCO_2$ treatment. The treatment is able to completely eliminate the hysteresis of the PVA OFETs and also significantly reduce the device subthreshold slope to a very low number of 0.25 V/dec while boosting the saturation regime carrier mobility to a very high number of 30.2 cm^2 V^{-1} s^{-1}. Both of these numbers are quite remarkable for flexible OFETs with polymer dielectrics. We further demonstrate that, coupling with an organic light-emitting diode (OLED), the OFET using the $SCCO_2$-treated PVA dielectric is able to function very well under fast switching speed, which suggests that this $SCCO_2$ approach is of high promise for future applications in organic electronics, especially for high refresh rate flexible display devices.

2. Results

Standard bottom-gate/top-contact OFET devices were used to prove the concept in this work. The devices used 2,7-dioctyl[1]benzothieno[3,2-b][1]benzothiophene (C8-BTBT) as the representative organic semiconductor and PVA as the polymer dielectric. The fabrication process of the devices is schematically illustrated in Figure 1(a), where a ~340 nm PVA layer was first spin-coated on a Si substrate, and then, the layer was treated with supercritical CO_2 fluid (i.e., $SCCO_2$ treatment) at 120°C under 3000 psi for 1 hour with the additive of anhydrous calcium chloride as the desiccant. The OFET devices were then completed by sequential evaporation of the C8-BTBT semiconductor and Au source/drain metal contacts. For comparison purposes, we also fabricated the OFET devices with alternative dielectrics of the untreated

(as spin-coated) PVA, air-annealed PVA (at 120°C for 1 h), and sequentially air-annealed and $SCCO_2$-treated PVA.

The electrical performance of the fabricated OFET devices was carefully characterized, and representative transfer characteristics in the saturated region are compared in Figures 1(b) and 1(c). The transfer characteristics were measured by sweeping the gate voltage (V_G) from +3 V (off-state) to −15 V (on-state) and then back to +3 V, while keeping fixed the drain voltage (V_D) at −15 V for generating saturated drain current (I_D) (Figure S1). As shown in Figure 1(b), pronounced hysteresis in the I_D-V_G curve appeared for the devices using the untreated PVA dielectric, whereas the hysteresis was greatly remedied by the $SCCO_2$ treatment on the PVA dielectric. To quantify the hysteresis, we extracted the threshold voltages (V_{th}) for both the forward and backward V_G sweeps and took their difference (ΔV_{th}) as a measure of the hysteresis. With the statistical analysis over 20 devices, we found that ΔV_{th} was fairly large as 5.55 ± 2.60 V for the untreated PVA devices and it became virtually zero (0.00 ± 0.02 V) by the addition of the $SCCO_2$ treatment. In contrast, conventional air annealing of the PVA dielectric did not improve the hysteresis at all, as ΔV_{th} remained at 5.72 ± 0.50 V for the air-annealed devices (Figure 1(c)). Notably, we also found that if the same $SCCO_2$ treatment was carried out after the air-annealing step, the hysteresis could also be improved to some extent (ΔV_{th} reduced to 1.52 ± 0.34 V) but not as much as that without the air-annealing step (Figure 1(c)). These numbers along with other device characteristics are summarized in Table S1.

The $SCCO_2$ treatment was also found to significantly improve the subthreshold slope of the devices. The subthreshold slope (SS) is defined as SS = $dV_G/d(\log_{10} I_D)$, which reflects the increase of V_G needed to generate one order of magnitude increase in the drain current. Certainly, a low SS is favored for the device operation with low voltage, high switching speed, and low power consumption. As shown in Figure 1(b) and Table S1, the devices with the untreated PVA dielectric exhibited a fairly large SS of 2.25 ± 0.51 V/dec. By adopting the $SCCO_2$ treatment, the SS value was significantly improved to 0.43 ± 0.21 V/dec, which is a remarkably low number for polymer-dielectric OFETs. In contrast, conventional air annealing could only reduce the SS value to some extent, and the residual SS was still high (1.29 ± 0.41 V/dec). If the $SCCO_2$ treatment was conducted after the air annealing, not much further improvement in SS could be obtained (0.93 ± 0.25 V/dec). The $SCCO_2$ treatment could also improve both on- and off-state drain currents (I_{on} and I_{off}). Compared to the devices using the untreated PVA, the $SCCO_2$-treated devices showed an enhanced I_{on} from 126 ± 14 to 160 ± 8 μA (at V_G = −15 V) and a suppressed I_{off} from 2.0 × 10^{-8} to 4.8 × 10^{-9} A, and therefore, the I_{on}/I_{off} ratio was improved by approximately 5 times from 6.3 × 10^3 to 3.3 × 10^4. It is worth noting that although I_{off} could also be improved by air annealing, the promotion of I_{on} could only be achieved by the $SCCO_2$ treatment. In addition, the saturation regime carrier mobility (μ_{sat}) of the devices was also found to increase from 20.9 ± 4.8 to 22.1 ± 2.9 cm^2 V^{-1} s^{-1} by the $SCCO_2$ treatment, whereas the conventional air annealing did not
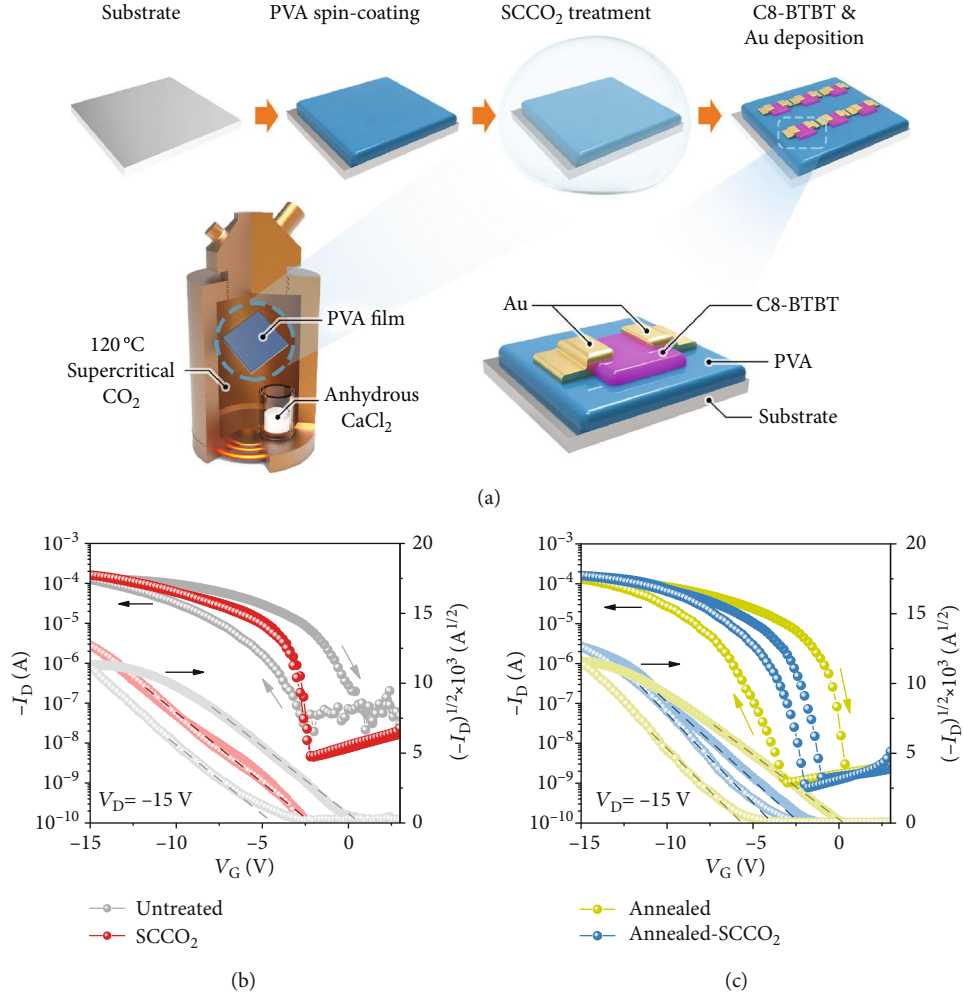
Figure 1: (a) Schematic illustration of the OFET device fabrication process, where the PVA dielectric is treated with supercritical CO_2 fluid. (b) Representative transfer characteristics of the OFET devices with untreated and $SCCO_2$-treated PVA dielectrics. (c) Representative transfer characteristics of the OFET devices with air-annealed and sequentially air-annealed and $SCCO_2$-treated PVA dielectrics.

appear to improve μ_{sat} (Table S1). It is worth noting that the extraction of the carrier mobility from the saturation regime (μ_{sat}) could possibly overestimate the numbers for high-mobility OFETs [37]; Choi et al. [38] recommended to look into the measurement reliability factor (r, see Methods) and calculate the corresponding effective carrier mobility (μ_{eff}), defined as $r \times \mu_{sat}$. Therefore, we also calculated the effective mobility for each OFET, and the number was found to also increase by the $SCCO_2$ treatment from 9.7 ± 3.2 to 14.0 ± 1.8 cm^2 V^{-1} s^{-1}, as compared to the untreated devices (Table S1). The bias stress stability of the OFETs was also tested, and the $SCCO_2$-treated devices exhibited much improved stability as compared to the untreated devices (Figure S2). To sum up the device characteristic results, we found that the $SCCO_2$ treatment could considerably improve the dielectric properties of PVA and therefore significantly enhance the device performance of OFETs. With the use of the $SCCO_2$-treated PVA dielectric, the OFET devices showed virtually zero hysteresis in I_D-V_G and a remarkably low SS of 0.43 V/dec, along with other appreciably improved parameters of I_{on}, I_{on}/I_{off} ratio, and μ_{sat}.

To further understand the associated mechanisms, we looked again at the direction of the I_D-V_G hysteresis for the untreated PVA devices. As shown in Figure 1(b), the hysteresis loop was in the clockwise direction, i.e., the current in the backward voltage sweep was higher than that in the forward sweep. Given this direction, the hysteresis was possibly originated from three sources [16], which are the polarization of the dielectric (ferroelectric or quasi-ferroelectric), charge injection from the gate electrode, and/or presence of mobile ions in the dielectric. The polarization of the dielectric was unlikely the reason because PVA is not a ferroelectric material [39]. The effect from the charge injection from the gate is usually prominent for thin dielectric layers (on the order of nanometers) [40] but unlikely to be significant for thick dielectrics as used in this case. Therefore, the presence of mobile ions in the dielectric seems to be the most likely dominating source for the hysteresis, and indeed, it has been used to explain the hysteresis in several other works [15, 16, 40]. To verify this mechanism, we fabricated metal-insulator-semiconductor (MIS) capacitor devices using the corresponding untreated and $SCCO_2$-treated PVA as the dielectric

layers and measured their dielectric spectra at various temperatures from 298 to 373 K. As displayed in Figure 2, the real part of the obtained dielectric permittivity (ε') and the loss tangent (tan δ) of the PVA dielectrics are plotted with respect to the frequency of the ac excitation voltage from 20 to 10^6 Hz. For the untreated PVA dielectric (Figure 2(a)), the ε' curve at 373 K is particularly large in the low-frequency region ($<10^2$ Hz), which signifies an additional relaxation channel for a slow responsive process [41, 42]. The tan δ curve at 373 K also shows a typical loss peak at 10^3 Hz for this process [41, 42]. The relaxation time of this slow process is consistent with the movement of mobile ions in a polymer matrix [40, 41], and the power law exponent of the imaginary part of the dielectric permittivity (ε'') further suggests that the ion movement was mixed of drifting and hopping (Figure S3). At lower temperatures (298~323 K), the ion movement became even slower, so the characteristic relaxation time was beyond the frequency range measured herein; nevertheless, the tan δ curve at 323 K shows some tail-like feature of a loss peak. As for the SCCO$_2$-treated dielectric (Figure 2(b)), the change of ε' with temperature and frequency is much smaller, and the tan δ curves show no loss peaks, which are consistent with the removal of the mobile ions by the SCCO$_2$ treatment. The mobile ions in polymers are usually monovalent ions, such as Na$^+$, K$^+$, and Li$^+$. In PVA, it is likely the Na$^+$ ions that cause the hysteresis issue, because NaOH is actually used in the synthesis of PVA from hydrolyzing poly(vinyl acetate), and therefore, it is very difficult to completely remove the Na$^+$ ions in the final product. The Na$^+$ ions remained in the PVA dielectric layer, causing the hysteresis in the OFET I_D-V_G response; as the SCCO$_2$ treatment removed the Na$^+$ ions, the hysteresis problem was therefore remedied.

The presence and removal of the Na$^+$ ions in the PVA layer were further confirmed by X-ray photoelectron spectroscopy (XPS) and by X-ray fluorescence spectrometry (XRF). Figure 3 displays the high-resolution XPS spectra of the Na 1s core-level emission for an as-spin-coated PVA film and the films subjected to each treatment as aforementioned. As shown in Figure 3, both the untreated and air-annealed PVA films exhibited a prominent Na 1s peak, and the peak intensity was greatly reduced by the SCCO$_2$ treatment. In particular, the Na XPS signal was below the noise level for the PVA film subject to only the SCCO$_2$ treatment (detection limit ~0.01 at.%). XRF was further used to quantify the Na contents inside the films. XRF measures the overall Na content throughout a film and is comparatively more accurate in quantifying metal elements. The Na contents were measured to be 141 ± 24, 172 ± 27, 4 ± 20, and 42 ± 21 ppm in mass for the untreated, air-annealed, SCCO$_2$-treated, and sequentially air-annealed and SCCO$_2$-treated PVA, respectively. These results clearly indicate that the SCCO$_2$ treatment was very effective in removing the Na$^+$ ions in the PVA film, as the Na content after the SCCO$_2$ treatment was barely observable by XRF. We also noticed that if the PVA film was first annealed, the thereafter SCCO$_2$ treatment became not as effective as before, possibly because the air annealing densified the PVA film and made some Na$^+$ ions locally trapped and inaccessible by the supercritical fluid.

Overall, the Na content was in positive correlation with the magnitude of the hysteresis (ΔV_{th}) as shown Figure 1. Therefore, these results well corroborate that the residual Na$^+$ ions in the PVA layer were the major origin for the I_D-V_G hysteresis and those ions could be well removed by the SCCO$_2$ treatment.

As for the subthreshold slope, it is known that SS is affected by the density of the charge traps at the semiconductor-insulator interface (D_{it}) and in the bulk of the semiconductor (D_{bulk}) via SS $= \ln (10)(kT/q)(1 + ((q \sqrt{\varepsilon_{SC}D_{bulk}} + q^2 D_{it})/C_i))$, where k, T, q, and C_i are, respectively, the Boltzmann constant, temperature, elementary charge constant, and the areal capacitance of the gate dielectric [43]. Provided that C_i was roughly the same before and after the SCCO$_2$ treatment (Table S2), it is likely that the charge trap density (D_{it} and/or D_{bulk}) was greatly reduced by the SCCO$_2$ treatment. The charge traps in PVA are probably from its hydroxyl groups, as they have been found to be efficient in trapping electrons and affect the device performance [26, 27]. To this end, we conducted XPS measurements to investigate the change of PVA upon the above treatments. Figure 4 displays the results of the XPS C 1s spectra for the untreated, air-annealed, SCCO$_2$-treated, and sequentially air-annealed and SCCO$_2$-treated PVA samples. All the spectra could be deconvoluted into four peak components at approximately 284.6, 286.0, 287.3, and 288.9 eV in binding energy, and these peak components could be assigned to the carbons in C–C/C=C, C–O, C=O, and O–C=O moieties, respectively [44]. As compared in Figure 4, both the air-annealing and SCCO$_2$ treatments reduced the C–O intensity and increased the C–C/C=C intensity, while the C=O and O–C=O intensities remained roughly unchanged. This observation is suggestive of a dehydration process, which removes the hydroxyl groups and converts C–O to C=C as schematically illustrated in Figure 4. The relative intensities of the C–O and C–C/C=C peak components are denoted above the peaks, and comparatively, the SCCO$_2$ treatment appears to be the most effective toward the dehydration, as the corresponding C–O and C–C/C=C intensities are, respectively, the lowest and highest among the others. The removal of the hydroxyl groups was also corroborated by Fourier-transform infrared spectroscopy (Figure S4), where the absorbance of the hydroxyl stretching mode was significantly reduced after the above treatments and the SCCO$_2$ treatment gave out the lowest hydroxyl absorbance. Although the detailed mechanisms for the SCCO$_2$ treatment being most efficient toward the dehydration are unknown and probably complex, we consider that the enhanced mass transfer of water by supercritical CO$_2$ fluid was likely to boost the dehydration reaction according to Le Chatelier's principle [31]. It is worth noting that the SCCO$_2$ treatment became ineffective post the air annealing, and this is perhaps because at the same time of dehydration the PVA chains also cross-linked and created some small isolated zones that trapped water from being further removed [45]. Nevertheless, the SCCO$_2$ treatment was the most effective in removing the electrically detrimental hydroxyls in PVA, which therefore considerably reduced the charge trap density and improved the subthreshold slope of the devices.
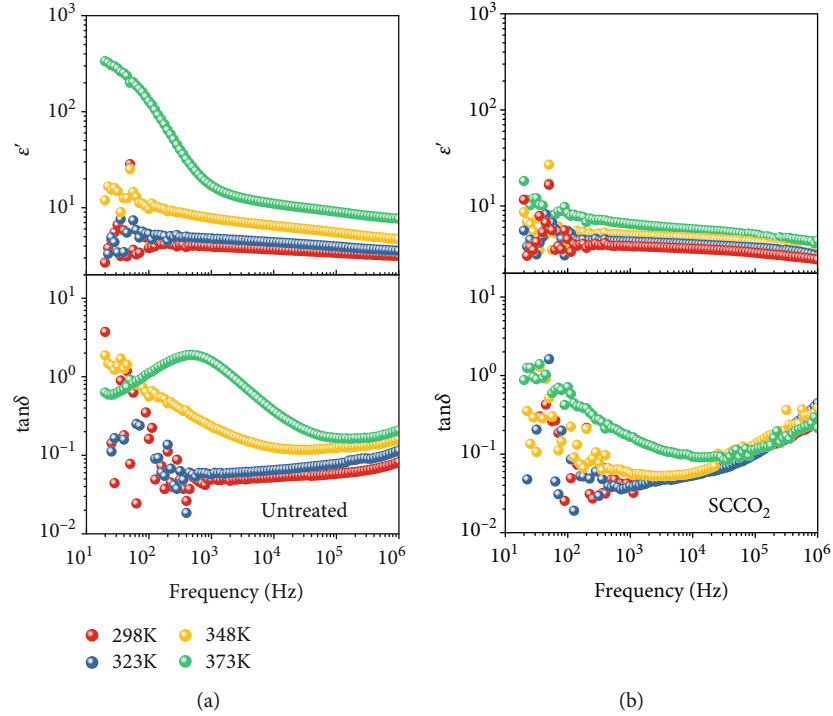
FIGURE 2: Dielectric spectra of (a) the untreated and (b) $SCCO_2$-treated PVA layers measured at various temperatures from 298 to 373 K.
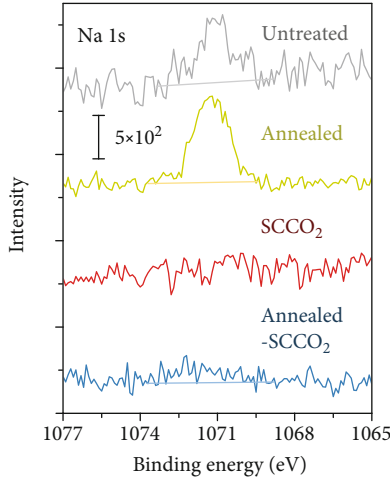

FIGURE 3: XPS Na 1s spectra of the untreated, $SCCO_2$-treated, air-annealed, and sequentially air-annealed and $SCCO_2$-treated PVA films.

In the following, we further demonstrate that the $SCCO_2$ approach is also well applicable to flexible OFET devices, which is of high technological importance for future applications. Although polymer dielectrics are ideal for flexible organic electronics, the problematic hysteresis associated with the polymer dielectrics has long been a critical issue that limits the switching speed, operation voltage, and power consumption of the OFET devices [13–16, 46, 47]. We herein used a piece of flexible transparent plastic coated with indium tin oxide (ITO) as the substrate and back gate and fabricated the same OFET devices on it, as shown in Figure 5(a). During

the device fabrication, the same treatments of air annealing, $SCCO_2$ treatment, and sequentially air annealing and $SCCO_2$ treatment were carried out on the PVA dielectrics, and the associated device performances (transfer characteristics) are shown in Figures 5(b) and 5(c). Similar to those shown in Figure 1, significant improvement in the device performance was also observed for the flexible OFETs: benefited from the $SCCO_2$ treatment, the hysteresis in the I_D-V_G curve was essentially removed ($\Delta V_{th} = 0.03 \pm 0.07$ V), the subthreshold slope was largely reduced to 0.25 ± 0.11 V/dec, I_{on} was enhanced to $158 \pm 28 \mu A$, I_{off} was reduced to 1.7×10^{-10} A, and therefore, the I_{on}/I_{off} ratio was significantly improved to 9.2×10^5 (Table S3). Notably, the SS and I_{on}/I_{off} numbers were even better than those on Si substrates, which is perhaps because the oxygen-rich ITO could also partially oxidize the hydroxyls and therefore reduced the charge trap density and suppressed the leakage pathway [48]. As a result, a very high saturation regime mobility (μ_{sat}) of 30.2 ± 4.6 cm^2 V^{-1} s^{-1} and a high effective mobility (μ_{eff}) of 13.8 ± 2.1 cm^2 V^{-1} s^{-1} were obtained, and these numbers considerably outperformed all previously reported flexible OFET devices, except for a recent work [49] which used single-crystal C8-BTBT as the organic semiconductor and reported a comparable carrier mobility (33.4 and 13.3 cm^2 V^{-1} s^{-1} for μ_{sat} and μ_{eff}, respectively) (Table S4). Given that the single crystal is considered to be the intrinsic limit for enhancing the mobility, our outcome relying on the improvement of the dielectric layer is quite remarkable in approaching to this limit.

As a further demonstration of the $SCCO_2$-prepared OFET devices for practical applications in organic electronics, we built a circuit using a $SCCO_2$-prepared OFET in series
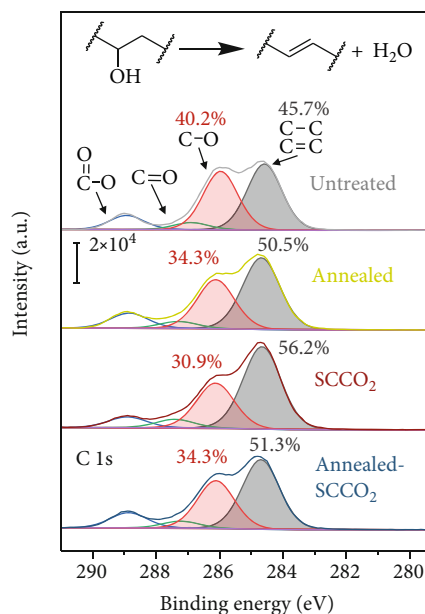
FIGURE 4: XPS C 1s spectra of the untreated, SCCO$_2$-treated, air-annealed, and sequentially air-annealed and SCCO$_2$-treated PVA films.

with a green-color OLED, where the OFET served as a switch to control the OLED (Figure 6(a)). As for demonstrative purposes, the green-color OLED was fabricated of a fairly large area of 16 mm^2, which is much larger than usual pixel size used in displays [50]; and therefore, as shown in Figure 6(b), the OLED needed a fairly large drive current of around 100 μA to achieve a luminance of 500 cd m^{-2} as needed for typical cell phone displays [51]. The circuit operation results are shown in Figures 6(c) and 6(d), where the current and luminance of the OLED are plotted against the gate voltage applied on the OFET, and the gate voltage was swept from 3 to −20 V and then back to 3 V. For comparison purposes, an OFET prepared with the untreated PVA dielectric was also used for these experiments, and the results are also plotted in Figures 6(c) and 6(d) for benchmarking. Clearly, significantly higher current and luminance along with much improved hysteresis were obtained for the OLED with the SCCO$_2$-treated OFET. Next, we supplied square-wave voltage alternating at 0 and −20 V (16 s in period) on the OFET gate to examine its switching behavior. Figure 6(e) compares the traces of the OLED luminance, and the associated video is provided as Supplementary Video 1. Clearly, the OLED coupled with the SCCO$_2$-treated OFET exhibited better performance in both the luminance and switching speed. A closer comparison of the snapshots taken at 0.03 and 0.16 s after switching V_G (Figure 6(f)) clearly shows that the untreated OFET resulted in apparent delay of light emitting when turning on and presence of ghost image when turning off, but these problems were not present for the SCCO$_2$-treated OFET. Another set of experiments was carried out using a much faster alternation speed for V_G, i.e., 5 Hz square wave (0.2 s in period). The associated

video is provided as Supplementary Video 2, and a number of the snapshots taken at various times are comparatively shown in Figure 6(g). Apparently, the untreated OFET was not able to follow the fast switching of V_G as the ghost image persisted throughout the entire off duration; and this problem was well conquered by the SCCO$_2$ treatment as no such ghost image appeared for the SCCO$_2$-treated device. All these above results clearly demonstrated that the SCCO$_2$ treatment was very effective to significantly improve the switching behavior of the OFETs for display control applications. Considering that OFETs are of the core units in a huge variety of contemporary organic circuits, we envision that this SCCO$_2$ technology will have a very broad spectrum of applications for organic electronics, especially for high refresh rate and low-voltage flexible display devices.

3. Discussion

In summary, we developed a new approach of using supercritical CO$_2$ fluid (SCCO$_2$) treatment on PVA dielectrics to achieve remarkably high-performance polymer-dielectric OFETs. Using C8-BTBT as the representative OFET semiconductor material, we demonstrated that the SCCO$_2$ treatment on PVA was able to completely eliminate the hysteresis in the OFET transfer I_D-V_G curves, which is a very critical issue for polymer-dielectric OFETs in general. Meanwhile, the treatment could also significantly reduce the OFET subthreshold slope and improve the on/off currents and carrier mobility. Detailed mechanism studies suggested that the effective elimination of the hysteresis and significant reduction of the subthreshold slope were because of the efficient removal of the mobile Na$^+$ ions and hydroxyl groups by the supercritical CO$_2$ fluid. We further showed that this SCCO$_2$ approach was also well applicable to flexible OFETs, where not only was the I_D-V_G hysteresis successfully removed but we were also able to achieve a very low subthreshold slope of 0.25 V/dec with a very high saturation regime carrier mobility of 30.2 cm^2 V^{-1} s^{-1}, and both of these numbers are quite remarkable for the flexible OFETs with polymer dielectrics. We further demonstrated that, coupling with an OLED, the SCCO$_2$-treated OFET was able to function very well under a fast switching speed of 5 Hz, which clearly indicated that an excellent switching behavior of polymer-dielectric OFETs could be enabled by this SCCO$_2$ approach. Considering that OFETs are of the core units in a huge variety of contemporary organic circuits, we envision that this SCCO$_2$ technology will have a very broad spectrum of applications for organic electronics, especially for high refresh rate and low-voltage flexible display devices.

4. Materials and Methods

4.1. Device Fabrication. To fabricate OFETs, heavily doped p-type Si wafers or ITO-coated polyethylene terephthalate (PET) plastic sheets were used as the bottom-gate substrates. The substrates were first cleaned by sequentially ultrasonicating in acetone, isopropanol, and deionized water for 20 min each and then treated with UV/ozone for 15 min. The PVA dielectric layer was prepared by spin
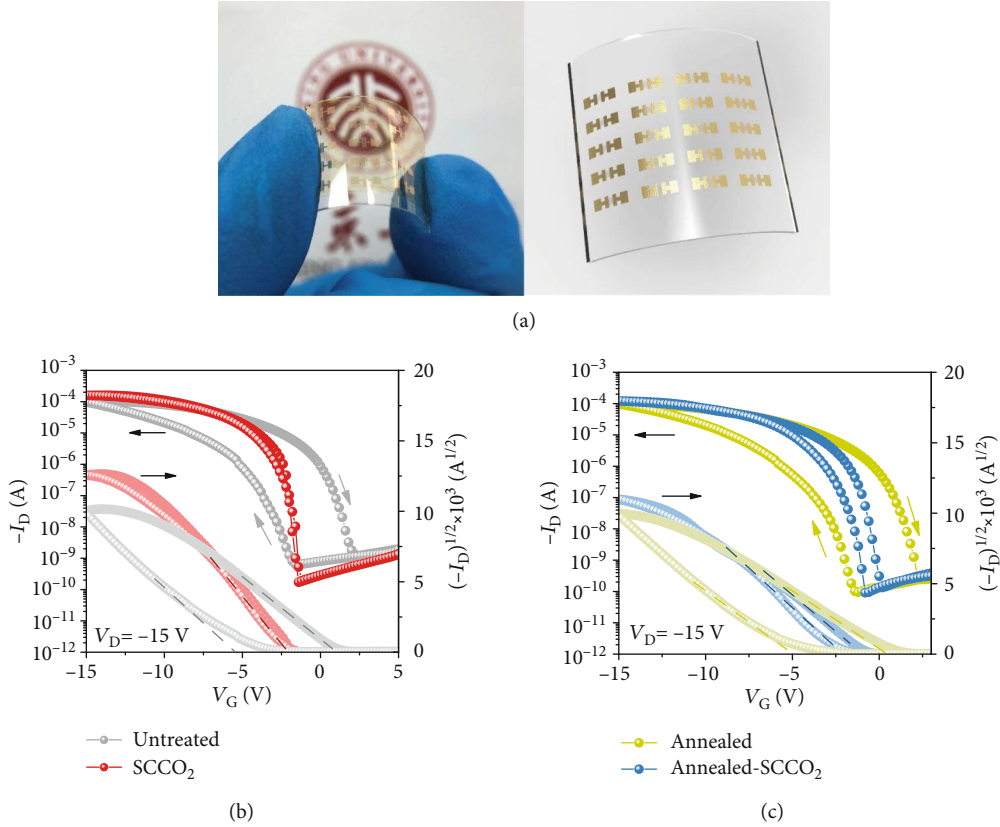
(a)

(b)

(c)

FIGURE 5: (a) Photographs of the OFETs prepared on a flexible transparent ITO-coated plastic substrate. (b) Transfer characteristics of the flexible OFETs with untreated and SCCO$_2$-treated PVA dielectrics. (c) Transfer characteristics of the flexible OFETs with air-annealed and sequentially air-annealed and SCCO$_2$-treated PVA dielectrics.

coating a PVA solution on the substrates at a speed of 3000 rpm. The PVA solution was prepared by first dissolving PVA solid particles (Mowiol® 40-88, 205,000 in molecular weight, Sigma-Aldrich) in deionized water (7.0 wt.%) at 70°C for 4 h and then adding ammonium dichromate (10 wt.% of PVA) for cross-linking. The PVA layer was then treated with supercritical CO$_2$ fluid with the additive of anhydrous calcium chloride as the desiccant at 120°C under 3000 psi for 1 h (i.e., SCCO$_2$ treatment). For comparison purposes, the PVA layer was alternatively annealed in air at 120°C for 1 h or sequentially annealed in air and then subjected to the same SCCO$_2$ treatment as above. In addition, the as-spin-coated PVA (i.e., untreated PVA) was also used for comparison. The organic semiconductor layer (30 nm) of 2,7-dioctyl[1]benzothieno[3,2-b][1]benzothiophene (C8-BTBT) was prepared by thermal evaporation at a deposition rate of 0.5 Å s^{-1} under chamber base pressure of 2×10^{-6} Torr. The OFET devices were then completed by thermal evaporation of 50 nm Au via a shadow mask to define the source and drain regions. The channel length and width of the OFETs were 100 μm and 1000 μm, respectively. The green-color OLEDs were fabricated following a previous report [52]. The layer structure of the OLED was

ITO/HATCN (5 nm)/N,N'-bis(naphthalen-1-yl)-N,N'-bis(phenyl)-benzidine (30 nm)/N,N-bis(4-(dibenzo[b,d]-furan-4-yl)phenyl)[1,1':4',1''-terphenyl]-4-amine (10 nm)/DMIC-CZ:DMIC-TRZ:Ir(ppy)$_2$acac (40 nm)/ANT-BIZ (70 nm)/Liq (2.5 nm)/Al (100 nm), and the layers were sequentially deposited by thermal evaporation. MIS capacitors were also prepared on the heavily doped Si wafer with the aforementioned PVA dielectrics. The bottom Si served as the bottom electrodes, and the top electrodes were 500 μm diameter circles of 50 nm thick Au, which were prepared by thermal evaporation via a shadow mask.

4.2. Characterizations. The electrical characterizations of the OFETs were carried out on a standard probe station with a Keysight B1500A semiconductor device analyzer in ambient air. Field-effect hole mobility in saturation regime (μ_{sat}) and threshold voltage (V_{th}) were extracted via the relation $I_D = -(W/2L)\mu_{FE}C_i(V_G - V_{th})^2$, where W, L, and C_i are the channel width, channel length, and areal capacitance of the gate dielectric, respectively. The effective carrier mobility (μ_{eff}) was calculated by $\mu_{eff} = r \times \mu_{sat}$, where r is the reliability factor defined as [38] $r = [(\sqrt{|I_{on}|} - \sqrt{|I_{off}|})/|V_G|^{max}]^2/((WC_i/2L)\mu_{sat})$. The dielectric spectra were measured by a Keysight
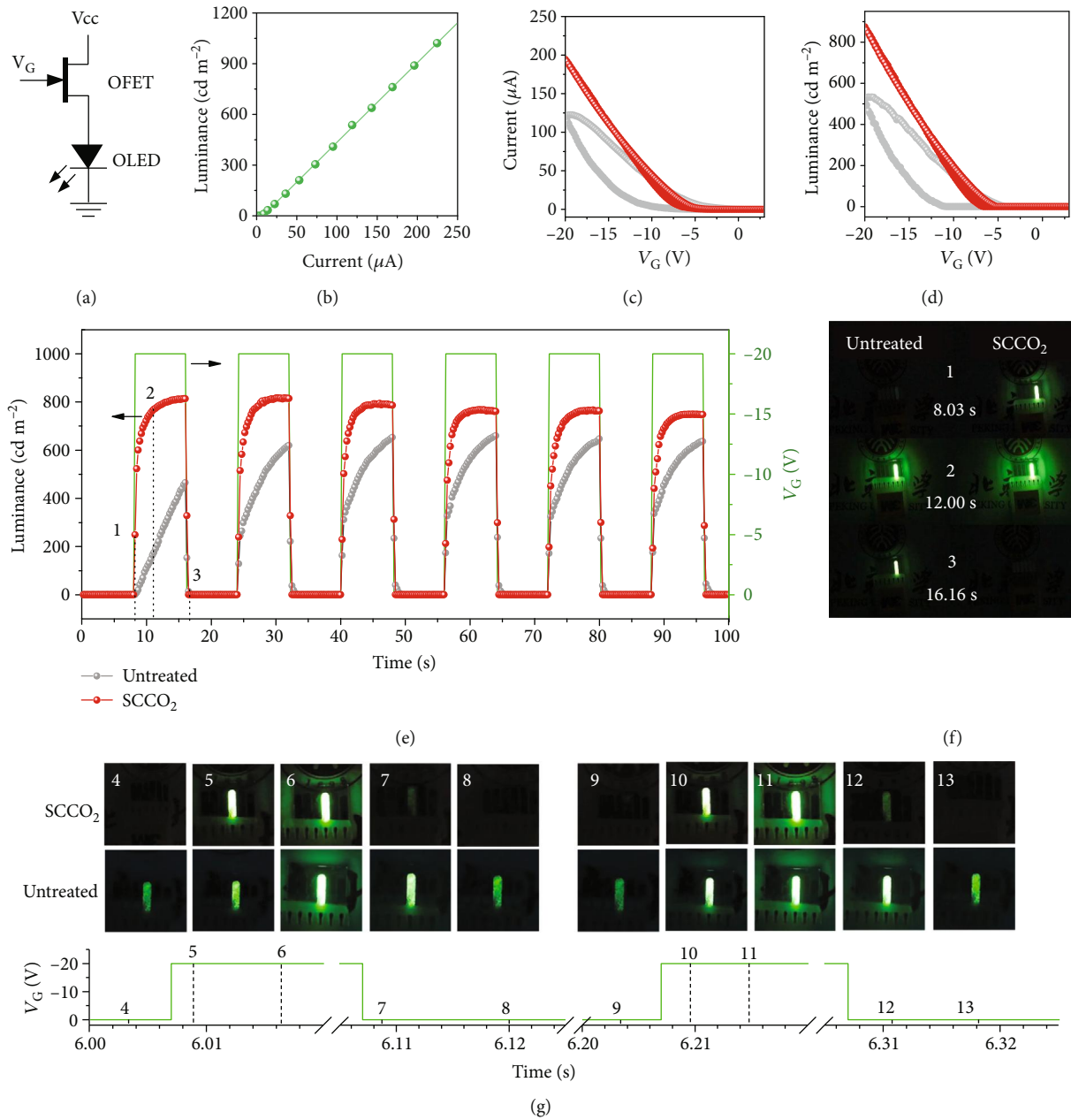
(a) (b) (c) (d)

(e) (f)

(g)

Figure 6: (a) Circuit diagram showing an OFET in series with an OLED. (b) Luminance of the OLED as the function of the drive current. (c) Current and (d) luminance as the functions of the gate voltage applied on the OFETs ($V_{CC} = -30$ V). The OFETs were fabricated with untreated and $SCCO_2$-treated PVA dielectrics. (e) Traces of luminance with time and (f) representative snapshots showing the switching behaviors of the OFETs upon square-wave V_G of 16 s in period. (g) Snapshots of the OLED upon faster switching V_G of 0.2 s in period (i.e., 5 Hz square wave). The corresponding time points are illustrated in the bottom curve.

E4980A LCR meter on the MIS capacitors with series resistance corrected. The luminance of the OLEDs was measured by a TOPCON BM-7AS luminance colorimeter. To characterize the material properties of the PVA layer, we used XPS (Thermo Scientific, Escalab 250Xi), XRF (Rigaku, ZSX Primus II), and Fourier-transform infrared spectroscopy (FTIR) (PerkinElmer, Frontier), and the layer thickness was measured by a stylus profiler (KLA Tencor, D-600).

Conflicts of Interest

The authors declare that there is no conflict of interest regarding the publication of this article.

Acknowledgments

Supplementary Materials

Figure S1: representative output characteristics of the OFET devices with (a) untreated, (b) SCCO$_2$-treated, (c) air-annealed, and (d) sequentially air-annealed and SCCO$_2$-treated PVA dielectrics. Figure S2: comparison of the bias stress stability of the OFET devices with (a) untreated and (b) SCCO$_2$-treated PVA dielectrics. During the bias stress test, the gate voltage was biased at –20 V, and the transfer characteristic was measured for every 5 min. Table S1: summary of the device characteristics for the PVA OFETs fabricated on Si substrates. The statistics were obtained based on the analysis over 20 devices. Figure S3: imaginary part of the dielectric permittivity (ε'') of the untreated PVA (at 373 K). Table S2: thickness (d) and areal capacitance (C_i) of the gate dielectric upon various treatments. Figure S4: FTIR spectra of the untreated, SCCO$_2$-treated, air-annealed, and sequentially air-annealed and SCCO$_2$-treated PVA films. Table S3: summary of the device characteristics for the PVA OFETs fabricated on flexible ITO-coated plastic substrates. Table S4: comparison of the device performance of the reported flexible OFETs using polymer dielectrics. Table S5: comparison of the device performance of the reported OFETs using the C8-BTBT semiconductor. Supplementary Video 1: switching behavior of the OFET-OLED circuit under the square-wave V_G of 16 s in period. Supplementary Video 2: switching behavior of the OFET-OLED circuit under the square-wave V_G of 0.2 s in period (i.e., 5 Hz square wave). (Supplementary Materials)

References

[1] T. Someya, Z. Bao, and G. G. Malliaras, "The rise of plastic bioelectronics," *Nature*, vol. 540, no. 7633, pp. 379–385, 2016.

[2] Y. Qian, X. Zhang, L. Xie et al., "Stretchable organic semiconductor devices," *Advanced Materials*, vol. 28, no. 42, pp. 9243–9265, 2016.

[3] Y. van de Burgt, A. Melianas, S. T. Keene, G. Malliaras, and A. Salleo, "Organic electronics for neuromorphic computing," *Nature Electronics*, vol. 1, no. 7, pp. 386–397, 2018.

[4] Y. Wen, Y. Liu, Y. Guo, G. Yu, and W. Hu, "Experimental techniques for the fabrication and characterization of organic thin films for field-effect transistors," *Chemical Reviews*, vol. 111, no. 5, pp. 3358–3406, 2011.

[5] H. Zhu, E.-. S. Shin, A. Liu, D. Ji, Y. Xu, and Y.-. Y. Noh, "Printable semiconductors for backplane TFTs of flexible OLED displays," *Advanced Functional Materials*, vol. 30, no. 20, article 1904588, 2020.

[6] C.-F. Liu, X. Liu, W.-Y. Lai, and W. Huang, "Organic light-emitting field-effect transistors: device geometries and fabrication techniques," *Advanced Materials*, vol. 30, no. 52, article 1802466, 2018.

[7] A. Yamamura, S. Watanabe, M. Uno et al., "Wafer-scale, layer-controlled organic single crystals for high-speed circuit operation," *Science Advances*, vol. 4, no. 2, article eaao5758, 2018.

[8] S. G. Higgins, T. Agostinelli, S. Markham, R. Whiteman, and H. Sirringhaus, "Organic diode rectifiers based on a high-performance conjugated polymer for a near-field energy-harvesting circuit," *Advanced Materials*, vol. 29, no. 46, article 1703782, 2017.

[9] P. C. Y. Chow and T. Someya, "Organic photodetectors for next-generation wearable electronics," *Advanced Materials*, vol. 32, no. 15, article 1902045, 2020.

[10] O. Knopfmacher, M. L. Hammock, A. L. Appleton et al., "Highly stable organic polymer field-effect transistor sensor for selective detection in the marine environment," *Nature Communications*, vol. 5, no. 1, p. 2954, 2014.

[11] A. Chortos, J. Liu, and Z. Bao, "Pursuing prosthetic electronic skin," *Nature Materials*, vol. 15, no. 9, pp. 937–950, 2016.

[12] X. Yu, W. Shou, B. K. Mahajan, X. Huang, and H. Pan, "Materials, processes, and facile manufacturing for bioresorbable electronics: a review," *Advanced Materials*, vol. 30, no. 28, article 1707624, 2018.

[13] B. Wang, W. Huang, L. Chi, M. al-Hashimi, T. J. Marks, and A. Facchetti, "High- k gate dielectrics for emerging flexible and stretchable electronics," *Chemical Reviews*, vol. 118, no. 11, pp. 5690–5754, 2018.

[14] Y. Wang, X. Huang, T. Li, L. Li, X. Guo, and P. Jiang, "Polymer-based gate dielectrics for organic field-effect transistors," *Chemistry of Materials*, vol. 31, no. 7, pp. 2212–2240, 2019.

[15] M. Egginger, M. Irimia-Vladu, R. Schwödiauer et al., "Mobile ionic impurities in poly(vinyl alcohol) gate dielectric: possible source of the hysteresis in organic field-effect transistors," *Advanced Materials*, vol. 20, no. 5, pp. 1018–1022, 2008.

[16] M. Egginger, S. Bauer, R. Schwödiauer, H. Neugebauer, and N. S. Sariciftci, "Current versus gate voltage hysteresis in organic field effect transistors," *Monatshefte für Chemie - Chemical Monthly*, vol. 140, no. 7, pp. 735–750, 2009.

[17] H. T. Yi, M. M. Payne, J. E. Anthony, and V. Podzorov, "Ultra-flexible solution-processed organic field-effect transistors," *Nature Communications*, vol. 3, no. 1, p. 1259, 2012.

[18] G. Gelinck, P. Heremans, K. Nomoto, and T. D. Anthopoulos, "Organic transistors in optical displays and microelectronic applications," *Advanced Materials*, vol. 22, no. 34, pp. 3778–3798, 2010.

[19] X. Guo, Y. Xu, S. Ogier et al., "Current status and opportunities of organic thin-film transistor technologies," *IEEE Transactions on Electron Devices*, vol. 64, no. 5, pp. 1906–1921, 2017.

[20] M. Noda, N. Kobayashi, M. Katsuhara et al., "An OTFT-driven rollable OLED display," *Journal of the Society for Information Display*, vol. 19, no. 4, pp. 316–322, 2011.

[21] T. Someya, M. Kaltenbrunner, and T. Yokota, "Ultraflexible organic electronics," *MRS Bulletin*, vol. 40, no. 12, pp. 1130–1137, 2015.

[22] H. Ren, N. Cui, Q. Tang, Y. Tong, X. Zhao, and Y. Liu, "High-performance, ultrathin, ultraflexible organic thin-film transistor array via solution process," *Small*, vol. 14, no. 33, article 1801020, 2018.

[23] C. J. Bettinger and Z. Bao, "Organic thin-film transistors fabricated on resorbable biomaterial substrates," *Advanced Materials*, vol. 22, no. 5, pp. 651–655, 2010.

[24] A. R. V. Benvenho, W. S. Machado, I. Cruz-Cruz, and I. A. Hümmelgen, "Study of poly(3-hexylthiophene)/cross-linked poly(vinyl alcohol) as semiconductor/insulator for application in low voltage organic field effect transistors," *Journal of Applied Physics*, vol. 113, no. 21, article 214509, 2013.

[25] C. A. Lee, D. W. Park, S. H. Jin, I. H. Park, J. D. Lee, and B.-G. Park, "Hysteresis mechanism and reduction method in the bottom-contact pentacene thin-film transistors with cross-linked poly(vinyl alcohol) gate insulator," *Applied Physics Letters*, vol. 88, no. 25, article 252102, 2006.

[26] M.-H. Yoon, C. Kim, A. Facchetti, and T. J. Marks, "Gate dielectric chemical structure–organic field-effect transistor performance correlations for electron, hole, and ambipolar organic semiconductors," *Journal of the American Chemical Society*, vol. 128, no. 39, pp. 12851–12869, 2006.

[27] S. Lee, B. Koo, J. Shin, E. Lee, H. Park, and H. Kim, "Effects of hydroxyl groups in polymeric dielectrics on organic transistor performance," *Applied Physics Letters*, vol. 88, no. 16, p. 162109, 2006.

[28] J. Shin, Y. Kim, Y. M. Lim, and Y. C. Nho, "Removal of sodium acetate in poly(vinyl alcohol) and its quantification by 1H NMR spectroscopy," *Journal of Applied Polymer Science*, vol. 107, no. 5, pp. 3179–3183, 2008.

[29] L. V. Smirnov, N. P. Kulikova, and N. V. Platonova, "Infrared spectra of polyvinylalcohol," *Polymer Science U.S.S.R.*, vol. 9, no. 11, pp. 2849–2856, 1967.

[30] X. Wang, S. Ochiai, G. Sawa et al., "Organic field-effect transistors with crosslinkable poly(vinyl alcohol) insulator and spin-coated/drop-cast poly(3-hexylthiophene-2,5-diyl) semiconductor," *Japanese Journal of Applied Physics*, vol. 46, no. 3B, pp. 1337–1342, 2007.

[31] L. M. Miller, J. D. Pinkston, and L. T. Taylor, *Modern Supercritical Fluid Chromatography*, John Wiley & Sons, Inc., 2019.

[32] J. W. King and L. L. Williams, "Utilization of critical fluids in processing semiconductors and their related materials," *Current Opinion in Solid State & Materials Science*, vol. 7, no. 4-5, pp. 413–424, 2003.

[33] R. Marr and T. Gamse, "Use of supercritical fluids for different processes including new developments—a review," *Chemical Engineering and Processing*, vol. 39, no. 1, pp. 19–28, 2000.

[34] C. A. Jones, A. Zweber, J. P. DeYoung, J. B. McClain, R. Carbonell, and J. M. DeSimone, "Applications of "dry" processing in the microelectronics industry using carbon dioxide," *Critical Reviews in Solid State and Materials Sciences*, vol. 29, no. 3-4, pp. 97–109, 2010.

[35] L. Li, K.-C. Chang, X. Lin, R. Zhang, and J.-H. Lou, "Insulating property improvement of polyimide in devices by low-temperature supercritical fluids," *Advanced Electronic Materials*, vol. 5, no. 12, article 1900580, 2019.

[36] J. Chrastil, "Solubility of solids and liquids in supercritical gases," *The Journal of Physical Chemistry*, vol. 86, no. 15, pp. 3016–3021, 1982.

[37] E. G. Bittle, J. I. Basham, T. N. Jackson, O. D. Jurchescu, and D. J. Gundlach, "Mobility overestimation due to gated contacts in organic field-effect transistors," *Nature Communications*, vol. 7, no. 1, p. 10908, 2016.

[38] H. H. Choi, K. Cho, C. D. Frisbie, H. Sirringhaus, and V. Podzorov, "Critical assessment of charge mobility extraction in FETs," *Nature Materials*, vol. 17, no. 1, pp. 2–7, 2018.

[39] Prateek, V. K. Thakur, and R. K. Gupta, "Recent progress on ferroelectric polymer-based nanocomposites for high energy density capacitors: synthesis, dielectric properties, and future aspects," *Chemical Reviews*, vol. 116, no. 7, pp. 4260–4317, 2016.

[40] V. Georgiou, D. Veksler, J. P. Campbell et al., "Ferroelectricity in polar polymer-based FETs: a hysteresis analysis," *Advanced Functional Materials*, vol. 28, no. 10, p. 1705250, 2018.

[41] R. J. Klein, S. Zhang, S. Dou, B. H. Jones, R. H. Colby, and J. Runt, "Modeling electrode polarization in dielectric spectroscopy: ion mobility and mobile ion concentration of single-ion polymer electrolytes," *The Journal of Chemical Physics*, vol. 124, no. 14, p. 144903, 2006.

[42] D. Fragiadakis, S. Dou, R. H. Colby, and J. Runt, "Molecular mobility, ion mobility, and mobile ion concentration in poly(ethylene oxide)-based polyurethane ionomers," *Macromolecules*, vol. 41, no. 15, pp. 5723–5728, 2008.

[43] B. Blülle, R. Häusermann, and B. Batlogg, "Approaching the trap-free limit in organic single-crystal field-effect transistors," *Physical Review Applied*, vol. 1, no. 3, p. 034006, 2014.

[44] D. Briggs, *Surface Analysis of Polymers by XPS and Static SIMS*, Cambridge University Press, 2009.

[45] H. S. Mansur, C. M. Sadahira, A. N. Souza, and A. A. P. Mansur, "FTIR spectroscopy characterization of poly (vinyl alcohol) hydrogel with different hydrolysis degree and chemically crosslinked with glutaraldehyde," *Materials Science and Engineering: C*, vol. 28, no. 4, pp. 539–548, 2008.

[46] Y. Yang, Z. Wang, Z. Xu et al., "Low hysteresis carbon nanotube transistors constructed via a general dry-laminating encapsulation method on diverse surfaces," *ACS Applied Materials & Interfaces*, vol. 9, no. 16, pp. 14292–14300, 2017.

[47] L. Tu, X. Wang, J. Wang, X. Meng, and J. Chu, "Ferroelectric negative capacitance field effect transistor," *Advanced Electronic Materials*, vol. 4, no. 11, article 1800231, 2018.

[48] S. Scholz, D. Kondakov, B. Lüssem, and K. Leo, "Degradation mechanisms and reactions in organic light-emitting devices," *Chemical Reviews*, vol. 115, no. 16, pp. 8449–8503, 2015.

[49] H. Chen, X. Xing, M. Zhu et al., "Low-voltage, high-performance flexible organic field-effect transistors based on ultrathin single-crystal microribbons," *ACS Applied Materials & Interfaces*, vol. 11, no. 37, pp. 34188–34195, 2019.

[50] H.-W. Chen, J.-H. Lee, B.-Y. Lin, S. Chen, and S.-T. Wu, "Liquid crystal display and organic light-emitting diode display: present status and future perspectives," *Light: Science & Applications*, vol. 7, no. 3, pp. 17168–17168, 2018.

[51] J. Souk, S. Morozumi, F. C. Luo, and I. Bita, *Flat Panel Display Manufacturing*, John Wiley & Sons, 2018.

[52] D. Fang, Y. Sun, Y. Chen et al., "Dibenzofuran-based iridium complexes as green emitters: realizing PhOLEDs with high power efficiency and extremely low efficiency roll-off," *Dyes and Pigments*, vol. 173, article 107990, 2020.